Electrochemical characteristics of BIS 2062 carbon steel under simulated ocean acidification scenario

K R Devika[1,2] and P Muhamed Ashraf [1*]

[1.] ICAR Central Institute of Fisheries Technology, Cochin 682 029, India

[2.] Kerala University of Fisheries and Ocean Studies, Cochin 682 025, India.

*** Corresponding Author**

Address

P Muhamed Ashraf, PhD

Principal Scientist

ICAR Central Institute of Fisheries Technology

Matsyapuri PO

Cochin 682 029.

Kerala, India

Email: ashrafp2008@gmail.com

Phone: +91 9746236477 (Mobil)

+ 91 484 2412300

Fax: +91 484 2668212

Miss. K R Devika

M Sc Student

Kerala University of Fisheries and Ocean Studies

ICAR Central Institute of Fisheries Technology

Matsyapuri PO

Cochin 682 029.

Kerala, India

Email: devikakr30@gmail.com

Electrochemical characteristics of BIS 2062 carbon steel under simulated ocean acidification scenario.

K R Devika[1,2] and P Muhamed Ashraf [1*]

[1] ICAR Central Institute of Fisheries Technology, Cochin 682 029, India

[2] Kerala University of Fisheries and Ocean Studies, Cochin 682 025, India.

Short Title: ***Impact of ocean acidification on steel***

Abstract

Climate change is always attributed to the rise in temperature and emission of gases like CO_2, and the latter is largely responsible for ocean acidification. The impact of ocean acidification is widely studied on marine organisms but not on the fate of marine materials exposed in the ocean. The present study aimed to assess the electrochemical characteristics of BIS 2062 boat building carbon steel due to the acidification of seawater. Electrochemical characteristics of steel were studied using acidified natural seawater (pH 8.05 to 6.50) as an electrolyte. Severe degradation of steel has occurred when the pH of seawater decreased from 8.05 to 7.90 thereby shifted the corrosion rate by 0.61 to 1.56 mm yr^{-1}. This was further aggravated with the severity of acidification. Results of the electrochemical impedance spectroscopy corroborated the findings of linear polarisation and also proved the formation of varied forms of FeOOH layers. The results strongly suggest the need for detailed study and redesign of marine materials in tune with ocean acidification.

Key words: ocean acidification, marine corrosion, carbon steel, seawater pH, EIS

1. Introduction

Climate change to a greater extent is attributed to the rise in temperature and emission of gases like carbon dioxide. The rise in temperature leads to global warming and emission of carbon dioxide to ocean acidification. The rapid dissolution of carbon dioxide in seawater decreases the pH of ~~the~~ seawater by increasing the H^+ ion concentration thereby reducing the carbonate ion formation, and hence saturation of biologically important calcium carbonate [1,2]. The whole process is described as ocean acidification. Fossil fuel combustion in the post-industrialization era has increased the proportion of carbon dioxide in the atmosphere and this, in turn, resulted in the drastic reduction of pH of oceanic surface waters [3-5]. Oceans act as a sink for 50% of the atmospheric CO_2 after post-industrialization and the same situation is still continued thereby rising the atmospheric CO_2 (pCO_2) level [6,7]. Marine ecosystems are

sensitive towards increased H^+ ion concentration, as it is distinctly evident from the dissolution of calcium carbonate from calcareous marine animals [8,9]. The secondary and tertiary impact is the changes in organic matter fluxes and the development of oxygen minimum zones [10]. Increased H^+ ion concentration not only enhances the dissolved HCO_3^- ions and reduces CO_3^{2-} but also decreases the unprotonated ligand-binding sites in the oceanic waters, this will decrease the binding of toxic and nutrient metals [11]. The reduction in carbonate ion concentration is normally associated with the decrease in buffering capacity and biologically available calcium carbonate in the ocean.

The post-industrialization era had added anthropogenic CO_2 in the ocean leading to a decrease in pH of 0.1 units throughout the globe [12], and this trend is being continued by a decrease in pH at the rate 0.002 unit yr^{-1} [13]. The rate varies in different regions depending on the buffering capacity of the seawater [14]. Fossil fuel and agriculture waste burning will enhance the production of strong acids like nitric and sulfuric acids in the atmosphere and also slightly influence the rate of ocean acidification [15]. LeQu´er´e et al. [12] described the pCO_2 after post-industrialization has reached a value of 400 μatm, out of which 120 μatm was added within the last 150 years. Interestingly, 50% of pCO_2 was emitted during the last 40 years. This was considered as the highest change in the atmosphere for the last 800000 years. The current addition of pCO_2 in the atmosphere is > 2 μatm yr^{-1} and never expected to bring down the pCO_2 level to 400 μatm [16]. Land and ocean plays an important role in attenuating the CO_2 generated anthropogenically and it was about 50% [17]. The largest reservoir is ocean surface which takes down to deeper layers due to ocean currents. Sea surface CO_2 equilibration takes about 6 months which is faster when compared with that was before 100 years. The major impact of ocean acidification, on calcified organism is the loss of shell thickness, density and strength [18-21]. The impact varies with organisms, shell parts and age of the shell [21]. Not much study has been conducted to understand the impact of ocean acidification in man-made structures like floating vessels and underwater structures.

Fishing boats are constructed mainly using BIS 2062 carbon steel, currently. The life of a fishing vessel is about 20 to 25 years. The fishers started experiencing the shortage of fish to harvest due to the impact of climatic changes and they are not much aware about the recent topics like ocean acidification, which is also a part of climate change. Material degradation due to acidification is an important challenge before them as most of the marine-grade steels were developed and designed to withstand the seawater pH ranging 8.00 to 8.50. It is important to

investigate the impact of ocean acidification on marine materials like steel. Liao et al [26] studied the fatigue due to pH and temperature and showed that the corrosive pH will decrease the fatigue life of Q345qD steel. Metal glassy alloys exposed in artificial seawater with varying pH inferred that the Cr content in the metal alloy has higher corrosion resistance than non-Cr alloys [23]. The hydrogen embrittlement study on TMCP 80 pipeline showed the hydrogen diffusion coefficients were increased with the increasing negative shift of potential in natural and acidic seawater [24]. Pitting corrosion was more evident in acidic seawater than natural seawater. Acidic pH and negative shift of potential helped to diffuse more hydrogen to the inner layers of the metal [24]. Acid-producing bacterial influence on corrosion over Q235 steel was studied and found that these bacteria form thick biofilm over the steel surface which enhanced the corrosion of the steel by forming an inner layer of Fe_3O_4 film [25]. Impact of ocean acidification on marine organisms was studied by flowing carbon dioxide gas to large tanks containing natural seawater. Mass flow controllers were used to optimize the CO_2 flow to attain the required pH in tanks. The oceanographic researchers relied on spectroscopic pH measurement in most of their experiments and it provides higher sensitivity than usual bulb pH measurement. Limited studies has been conducted by modifying the pH of natural seawater using CO_2 on corrosion characteristics of marine-grade metal alloys. The present study is carried out to understand the electrochemical characteristics of BIS 2062 carbon steel by exposing it in the natural seawater with varying pH.

2. Materials and methods

2.1. Materials

Surface seawater was collected from $10^0$00.557´N, $076^0$10.184´E off Cochin. Reagents like m-cresol purple dye and acetone were procured from Merck India Ltd. The carbon steel BIS 2062 was purchased from KSINC Boat yard Ernakulam. The carbon dioxide with 95% purity was sourced from Ernakulam. The steel coupon was polished by using SiC papers serially upto 1000 grits.

2.2. pH of sea water using spectrophotometer

The pH of the seawater was measured through spectrophometric method outlined by Dickson et al [26]. The pH of the seawater was determined by adding m-cresol purple in the seawater. The reaction is expressed as

$$HI^-(aq) = H^+(aq) + I^{2-}(aq) \quad \text{…… 1}$$

$$pH = pK(HI^-) + \log[I^{2-}]/[HI^-] \quad \text{…… 2}$$

Where I is the indicator dye. A detailed description of the principal and method is available in Dickson et al [26]. The spectrophotometric measurement of seawater is done by using Shimadzu 2450 double beam UV visible spectrophotometer by scanning the seawater in three wavelengths, viz., 730 nm form cresol purple, 578 nm as absorption maxima for the base and 434 nm absorption for the acid forms. Measured the UV-Vis absorption of the seawater without adding the dye and with 0.05 ml of 2 mmol l^{-1} dye solution having pH 7.9 ± 0.1 in a 10 cm long path cell. The absorption ratio of base and acid component (A_1/A_2) provides information on the extent of protonation due to dye. The spectrophotometer analysis was done after baseline correction and all measurements were carried out at 25 ± 2°C. The pH of the seawater was calculated using the equation

$$pH = pK_2 + \log_{10}(A_1/A_2 - X)/(Y - ((A_1/A_2)\,Z)) \quad \text{…….. 3}$$

Where

$X = \varepsilon_1(HI^-)/\varepsilon_2(HI^-) = 0.00691$

$Y = \varepsilon_1(I^{2-})/\varepsilon_2(HI^-) = 2.2220$

$Z = \varepsilon_2(I^{2-})/\varepsilon_2(HI^-) = 0.1331$

$pK_2 = (1245.69\ (T / K)) + 3.8275 + 0.00211(35 - S)$

ε is the extinction coefficient of different ionic species. A_1 and A_2 are the absorption maxima of base and acid forms. The equilibrium constant pK_2 is the function of salinity and temperature. Corrected (A_1/A_2) value to zero dye effect using equation 4. V is the volume of the dye solution pipetted. T/K is the temperature in K and S is the salinity in psu.

$$(A_1/A_2)corr = (A_1/A_2) - V[a + b(A_1/A_2)] \quad \text{…… 4}$$

$$= (A_1/A_2) - 0.05[0.125 - 0.147(A_1/A_2)]$$

Final pH was calculated using the equation by incorporating the constants and corrections using Microsoft Excel spreadsheets.

Seawater collected from the 10^0 00.557´N, $076^0$10.184´E of Kerala coast is used in this experiment. Salinity of the original seawater was determined to be 35.58 by using conductivity

meter. Seawater is acidified by passing the CO_2 gas from the carbon dioxide cylinder. Prepared the seawater having varied pH, viz., 7.9, 7.8, 7.7, 7.6, 7.5, 7.3, 7.0, and 6.5. and maintained by controlling the flow of CO_2 gas manually. Spectrophotometrically the pH was measured and the same was compared by using CRM calibrated glass electrode pH meter (Eutech Instruments Model. PC 2700). All the experiments were conducted at 25±2^oC.

2.3. Electrochemical studies

Electrochemical measurements were carried out by using Metrohm 302N Potentiostat with FRA2 impedance spectroscopy module. Ag/AgCl (3M KCl), platinum rod and BIS 2062 steel were used as reference, counter, and working electrode for measurement. Natural seawater with varied pH was used as the electrolyte. The linear polarization studies were carried out by exposing the steel in electrolyte for an hour and scanned 0.5 V ± of open circuit potential with a potential scan rate of 0.001 V s^{-1}. Tafel plots were drawn and data were derived by using Metrohm Nova software. Electrochemical impedance spectroscopic evaluation was carried out at open circuit potential after 30 min exposure in the electrolyte. The EIS scan was done from 100 kHz to 0.1 Hz at 6 decades. The resultant data were analyzed by using Nova software after fitting with the Randles equivalent circuit model. The whole experiment was repeated at least three times with fresh coupons at 25 ± 2^oC.

3. Results and discussion

3.1. Optimisation

The challenge was the acidification of natural seawater and optimization of CO_2 gas flow rate for getting the desired pH. The natural seawater pH used in the present study was 8.05 and the same water was used throughout the study. Prepared three different pH modified seawater, namely 7.90, 7.50, and 6.40. Monitored the change in pH with time due to the buffering capacity of seawater (Fig 1). The rate of change of pH was 0.004, 0.008 and 0.02 units per hour respectively for pH 7.90, 7.50 and 6.40. When pH was near to the original seawater pH (8.05), returning to the initial pH was a slow process, whereas the acidic pH, it quickly returned to the original pH. This indicated that the experiments carried out under low pH scenarios should be conducted with care due to faster pH variation. Compared the pH values of acidified seawater by using spectrophotometric and glass electrode pH meter methods. The pH recorded by the spectrophotometer and glass electrode pH meter covaried (Fig 1) and the pH value obtained from the spectrophotometer showed a little lower value than that obtained from glass electrode

pH meter. The linear relationship between the above instruments was y = 0.8761 x + 0.8726. In all our preceding experiments the reference pH was taken from spectrophotometry. It was not successful to optimize the CO_2 flow rate to maintain the specific pH for longer days in a smaller tank (5-10 liter), since the pH difference between the original seawater pH and experimental pH required was very narrow.

3.2. Linear sweep voltammetry

Corrosion of boat building, carbon steel BIS 2062 under varying pH was studied through linear polarization studies. The steel samples of 1 cm^2 area were exposed in the seawater having pH 8.05 to 6.5 with an accuracy of ±0.02. The linear sweep voltammetric data were presented in Fig 2. The corrosion potential (Ecorr), corrosion current density (Icorr), polarization resistance (Rp) and corrosion rate was ranged from -0.879 ± 0.009 to -0.829 ± 0.045 V, 5.287×10^{-5} ± 5.32×10^{-5} to 1.74×10^{-4} ± 7.15×10^{-5} A cm^{-2}, 2850 ± 1217 to 658 ± 359 Ohm cm^2 and 0.614 ± 0.618 to 2.420 ± 1.587 mm yr^{-1} respectively. The Ecorr values shifted towards the more cathodic side on decreasing the pH of the seawater. The lowest corrosion current density was shown at pH 8.05, it was increased with decreasing pH. The highest corrosion current density was exhibited at pH 7.00. Polarization resistance also followed a similar reverse pattern since they are inversely related. This indicated that the decrease in pH or ocean acidification makes the steel more stressful and susceptible to higher corrosion rate. 0.15 unit of pH decrease from 8.05 pH made about a 50% increase in corrosion current density and a 45% decrease in polarization resistance. This shows that the material will undergo severe corrosion by a small unit change of pH. The corrosion rate was also shown in a similar pattern. The corrosion rate was related to the corrosion current density and it was found that the rate of corrosion was increased from 0.61 mm yr^{-1} to 1.56 mm yr^{-1} by decreasing the pH from 8.05 to 7.90. Similarly, at pH 7.5 the corrosion rate increased to 2.26 mm yr^{-1}, and the value was 3 times higher than the current corrosion rate. The result showed an alarming scenario of marine materials under changing ocean pH. Since the pH of oceans already underwent 0.10 units lower after the post-industrialization era and currently, it has changed from 0.002 to 0.003 or higher unit per year [13, 27]. This implies that there will be an expected ~~a~~ change of seawater pH about 0.10 units in the next 1 to 2 decades. Generally the materials for marine purpose was designed to work the pH between 8.0 to 8.5. It is to note that the life of a steel boat is 20 to 25 years. The steel will undergo increased degradation year by year due to ocean acidification, since the pH was decreasing at the rate of pH 0.002 units. The changing climate scenario stressed to redesign

marine-grade steels to combat degradation. Electrochemical impedance spectroscopy evaluation can provide the mechanism of reaction due to ocean acidification.

3.3. Electrochemical impedance spectrometry

Electrochemical impedance spectroscopy of materials enables to understand the electrochemical characteristics of complex systems. The impedance experienced over an electrode is expressed as a complex number represented by a Nyquist plot where imaginary (-Z") vs real (Z') part can be plotted. Electrochemical impedance spectral characteristics of carbon steel were studied by exposing it in different seawater pH. The resulted data was fitted with simple Randle's equivalent circuit model (Rs (C1 [R1(R2C2)]) where Rs is the solution resistance, R1 and R2 was the polarization resistance at high and low-frequency domain and C1 and C2 are constant phase element (CPE) at high and low-frequency domain (Supplementary Fig S1). The CPE was incorporated for best fitting instead of an ideal capacitance. The CPE is expressed by

$$Zcpe = 1/ A(j\omega)^n$$

Where $j = (-1)^{1/2}$, angular frequency $\omega=2\pi f$, and A and n are frequency independent fit parameters. The n is CPE power, which varied from 0.5 to 1. When n = 0.5, it is Warburg impedance and n= 1 implies an ideal capacitance. All impedance plots in the current experiment exhibited n value almost equal to 1, which indicated an ideal capacitance. The high frequency (HF) domain of the Nyquist plot highlighted the charge transfer process and the low frequency (LF) domain was responsible for the mass transfer process. The results of the impedance spectra is presented in Fig 3. HF domain polarization resistance, R1, and constant phase elements, C1, varied from 45.23 ± 26.78 to 105.63 ± 25.25 Ohm cm^2 and $1.53\times10^{-09} \pm 6.45\times10^{-10}$ to $1.80\times10^{-8} \pm 1.52 \times10^{-8}$ F respectively. Whereas in the LF domain, the R2 and C2 respectively ranged from 156 ± 57.7 to 564 ± 171 and $1.1\times10^{-4} \pm 4.15 \times10^{-5}$ to $5.14 \times10^{-3} \pm 2.79 \times10^{-3}$ F. Two distinct semi-circle representing high and low-frequency domain showed the role of outermost and inner layers of the steel matrix. The higher diameter of low-frequency domain signifies the polarization resistance of the internal layer. Internal layer characteristics have a prominent role in corrosion inhibition. The fitted data highlighted that the outermost layer of the matrix exhibited higher polarization resistance and lowest capacitance. The increased polarization resistance in HF domain is due to the thickening of the outermost metal oxide film present in the matrix. This may be due to the effect of reduced pH and increased H^+ ion

concentration in the electrolyte solution [28]. The outermost layer tries to protect the matrix by preventing the attack of corrosives to the internal layers. The charge transfer and diffusion process are more simplified in the outermost layer because this layer was very weak, porous and highly susceptible to corrosion in aggressive environment [29].

Highest polarisation resistance (R2) in the low-frequency domain was showed at pH 8.05 and on acidification of the seawater, the steel exhibited decreased polarization resistance. Similarly, the capacitance was lowest for metal exposed in pH 8.05 and on acidification, the C2 was increased except in the case of metal exposed in pH 7.0 electrolyte. On decreasing the pH, the internal layers of the steel matrix underwent higher stress due to the presence of increased H^+ ions and hence the lower polarization resistance. This may probably due to increased thickness of the outermost layer, however, the layer has more cracks and pores [29]. This enabled the penetration of corrosives into the internal layers leading to degradation. The results were corroborating with the results of linear sweep voltammetry data. Nyquist plots of all the samples in different pH exhibited interesting Nyquist curves (Fig 4). The pH 8.05, 7.90, 7.80 and 7.70 exhibited Nyquist plots with two distinct HF and LF domains. The intersection of HF and LF showed a V-shaped curve with wider angles than pH 8.05. Among them highest was 55°, exhibited at pH 7.90, and this showed the internal layer and outer layer has low interaction and independent behavior (Supplementary Figure S2). Further reduction of pH to 7.6 and 7.5 exhibited the development of a medium frequency domain immediately after the HF curve apart from HF and LF. The angle between HF and LF was 60 and 52^o respectively and the intersection was V-shaped with a wider tilt towards the LF region side, due to the formation of a medium frequency domain. This showed the development of a new corrosion product layer with different molecular characteristics formed along with the internal layers. This layer might be denser with continuous low-density cracks and pores [29]. This led to the accumulation of chloride ions near this layer and hence the internal matrix layer was highly susceptible to corrosion [30]. The HF region exhibited two fragmented curves due to further decrease of pH to 7.30, 7.00, and 6.50 and these indicated two different molecular characteristics in the outermost layer. The angle between HF and LF was 65, 43 and 54° respectively. The HF and LF intersection were not conical instead a wider base (U shaped), which clearly inferred that the two outermost thin film layers are independent and have no interaction with the internal matrix (Supplementary Fig S2). Probably the above said new medium frequency domain layer in the internal matrix was moved up and joined with the outermost layer [29,30]. The Nyquist plot of pH 7 was specific and it was different from the other pH. The medium frequency domain

and inductance behavior represented the adsorption of the oxygen-derived intermediate on the cathode or CO poisoning on the anode[31] due to the lower pH.

3.4. Mechanism of corrosion

The boat building steel BIS 2062 underwent increased corrosion on acidification of seawater. The steel surface has a natural mill scale comprised of iron (II and III) oxides. This outermost layer has cracks and pores, and highly susceptible to corrosion in aggressive marine environments. On reducing the pH of the seawater OH^- ion concentration decreases and increases the H^+ ion concentration in the seawater electrolyte, this enabled the thickening of outermost layer with β-FeOOH and partly γ-FeOOH [32]. The electrochemical process involved was anodic liberation of Fe ion and cathodic reduction of H^+ ion. The steel matrix was covered with Fe (III or II) oxides Fe_3O_4 or Fe_2O_3 and then Fe^{2+} was hydrolyzed to FeOOH, mainly β and γ forms. This layer has prevented the intrusion of corrosive Cl^- ion which was clearly evidenced by the higher polarization resistance [29], and the phenomenon has shorter life. Further lowering of pH of seawater, led to the formation of a thin inner layer of α-FeOOH ~~was formed~~ just above the internal matrix due to the increased H^+ ion concentration.[29] Its composition was similar to akageneite [29]. The result needs further studies to understand the exact composition. This layer facilitated the increased accumulation of Cl^- ions in the vicinity through slow penetration into the internal layer and hence increased corrosion. These results highlighted the unique behavior of carbon steel below pH 8.00 and it needs more attention as the ocean pH is decreasing year by year.

3.5. Impact of ocean acidification

Post industrialization era witnessed a decrease of 0.1 pH unit and expected a change of 0.1 unit from the next 1-2 decades [13,28]. Linear polarization studies showed a decrease in pH of 0.15 unit from the natural pH of seawater and exhibited 2.5 times higher corrosion rate than the present scenario. Similarly, 2.01, 1.58, 3.20, 3.70 and 3.30 times higher corrosion rate were obtained at 7.80, 7.70, 7.60, 7.50 and 7.30 pH respectively. This study implies that 1 cm thick carbon steel will disappear after 4 years if pH decreased from 0.15 to 0.30 units. Further decrease in pH can deteriorate ~~of~~ carbon steel faster. These results showed the urgent need to undertake research on the development of new materials, which can combat changing climate and ocean acidification. A large number of materials holding sensors, underwater pipelines,

cables, and artificial underwater habitats has already been deployed in World Ocean and stability of these materials are under risk in the coming decade due to ocean acidification.

3.6. Conclusions

Climate change is largely attributed to the rise in temperature and the emission of gases like carbon dioxide. The rise in temperature leads to global warming and emission of carbon dioxide to ocean acidification. The impact of ocean acidification in BIS 2062 was evaluated by exposing the steel in varied seawater pH conditions. The results showed the corrosion rate was increased 2.54 times by changing pH from 8.05 to 7.90. The results were further affirmed by electrochemical impedance spectral studies. The corrosion rate of steel was increased due to the thickening of outer layer and further lowering in the pH can increase the interaction of H^+ ion with internal layers resulting in the formation of α-FeOOH. The study highlighted the immediate need for redesigning the marine steel alloys to mitigate ocean acidification. Further studies should be undertaken on the impact of ocean acidification on various metal alloys, and polymeric materials which are already been deployed in the ocean.

Acknowledgement

Authors thank the Director, ICAR - CIFT for the encouragement received to carry out the research. Also thanks are due to the technical and supporting staff of the Fishing Technology Division, ICAR – CIFT.

Conflict of interest

The authors declare that they have no conflict of interest.

Funding source

This research did not receive any specific grant from funding agencies in the public, commercial, or not-for-profit sectors**.**

Data availability

The data pertaining this paper will be available with the corresponding author. The data will be shared with reasonable request

Authors contributions

PMA conceptualized the idea, supervision of experiments, and writing of the manuscript.

KRD, standardization of the experimental procedures, analysis, and manuscript preparation.

4. References

1. Keeling CD, Bacastow RB, Bainbridge AE et al. (1976) Atmospheric carbon dioxide variations at mauna loa observatory, hawaii. Tellus 28(6): 538–551, doi:10.1111/j.2153-3490.1976.tb00701.x.

2. Jin P, Wang T, Liu N et al (2015) Ocean acidification increases the accumulation of toxic phenolic compounds across trophic levels. Nature Communications, 6: 8714, DOI: 10.1038/ncomms9714.

3. IPCC. Climate Change 2014: Impacts, Adaptation, and Vulnerability Part B: Regional Aspects. (eds Field, C. B. et al.) (Cambridge Univ. Press, 2014).

4. Stockdale A, Tipping E, Lofts S, Mortimer RJG (2016) Effect of Ocean Acidification on Organic and Inorganic Speciation of Trace Metals. Environ Sci Technol 50**:**1906−1913.

5. Steinacher M, Joos F, Frölicher TL, Plattner G-K, Doney SC (2009) Imminent ocean acidification projected with the NCAR global coupled carbon cycle-climate model. Biogeosciences Discuss 5: 4353–4393.

6. Sabine CL, Feely RA, Gruber N et al. (2004) The oceanic sink for anthropogenic CO2. Science, 305 (5682): 367−371.

7. Caldeira K, Wickett ME (2003) Anthropogenic carbon and ocean pH. Nature, , 425: 365.

8. Kleypas JA, Buddemeier RW, Archer D, Gattuso JP, Langdon C, Opdyke BN (1999) Geochemical consequences of increased atmospheric carbon dioxide on coral reefs. Science, 284 (5411): 118−120

9. Wootton JT, Pfister CA, Forester JD (2008) Dynamic patterns and ecological impacts of declining ocean pH in a high-resolution multi-year dataset. Proc. Natl. Acad. Sci. U. S. A., 105 (48*):* 18848−18853.

10. Hofmann LJ, H.-J. Schellnhuber, (2009) Oceanic acidification affects marine carbon pump and triggers extended marine oxygen holes. Proc. Natl. Acad. Sci. U. S. A.**,** 106 (9)**:** 3017−3022.

11. Hirose K (2011). Chemical modeling of marine trace metals: effects of ocean acidification to marine ecosystem. 2011 Seventh International Conference on Natural Computation. IEEE**.** 4**:** 2023−2026.

12. Le Qu´er´e, C. Andrew RM, Friedlingstein P et al. (2018) Global carbon budget 2017. Earth System Science Data, 10(1*)***:** 405–448 doi:10.5194/essd-10-405-2018

13. Bates NR, Astor YM, Church MJ, et al. (2007) A Time-Series View of Changing Surface Ocean Chemistry Due to Ocean Uptake of Anthropogenic CO_2 and Ocean Acidification. Oceanography 27(1):126-41.

14. Thomas H, Friederike Prowe AE, van Heuven S et al. (2007) Rapid decline of the CO2 buffering capacity in the north sea and implications for the North Atlantic Ocean. Global Biogeochemical Cycles, 21(4): doi:10.10[2/2006GB002825.

15. Doney SC, Mahowald N, Lima I, et al, (2007) Impact of anthropogenic atmospheric nitrogen and sulfur deposition on ocean acidification and the inorganic carbon system. Proceedings of the National Academy of Sciences, 104(37**):** 14580–14585 doi:10.1073/pnas.0702218104.

16. Betts RA, Jones CD, Knight JR, Keeling RF, Kennedy JJ (2016) El Ni˜no and a record CO2 rise. Nature Climate Change, 6**:** 806

17. Sabine CL, Feely RA, Gruber N et al. (2004) The oceanic sink for anthropogenic CO2. Science, 305 (5682): 367−371.

18. Nienhuis S, Palmer AR, Harley CDG. (2010) Elevated CO2 affects shell dissolution rate but not calcification rate in a marine snail. Proc. R. Soc. B Biol. Sci., 277**,** 2553–2558 doi: 10.1098/rspb.2010.0206

19. Rodolfo-Metalpa R, Houlbreque F, Tambutte E, et al. (2011)Coral and mollusc resistance to ocean acidification adversely affected by warming. Nat. Clim. Change**. 1,** 308–312. doi: 10.1038/nclimate1200

20. Queirós AM, Fernandes JA, Nunes J, et al. (2015) Scaling up experimental ocean acidification and warming research: from individuals to the ecosystem. Glob. Change Biol.**,** 21, 130–143 doi: 10.1111/gcb.12675

21. Chatzinikolaou E, Grigoriou P, Keklikoglou K, Faulwetter S, Papageorgiou N, Norkko J (2016) The combined effects of reduced pH and elevated temperature on the shell density of two gastropod species measured using micro-CT imaging. ICES J. Mar. Sci.**,** 74**,** 1135–1149 doi: 10.1093/icesjms/fsw219

22. Liao X, Huang Y, Qiang B, Yao C, Wei X, Li Y, (2020) Corrosion fatigue tests in synthetic seawater with constant temperature liquid circulating system. International Journal of Fatigue, 135: Article number 105542

23. Emran KM, Al-Harbi AK (2020) Impact of pH on the Corrosion of Novel Metal-Metal Glassy Alloys in Artificial Seawater: An Electrochemical and Morphology Study. Journal of Materials Engineering and Performance, 29(1): 175-181 (2020)

24. Li P, Geng Y, Hu R, Guo W, Peng W, Du M, Lin C (2019) Effect of ph value on hydrogen embrittlement of TMCP X80 steel in seawater. Biodiversity Science.**,** 31 (4**):** 387-395 Article number 1002-6495(2019)04-0387-09

25. Tian F, He X, Bai X, Yuan C (2020) Electrochemical corrosion behaviors and mechanism of carbon steel in the presence of acid-producing bacterium Citrobacter farmeri in artificial seawater. International Biodeterioration and Biodegradation, 147: Article number 104872

26. Dickson AG, Sabine CL, Christian JR (Eds.) Guide to Best Practices for Ocean CO2 Measurements. PICES Special Publication 3, pp 191 (2007)

27. Kapsenberg L, Alliouane S, Gazeau F, Mousseau L, Gattuso J.-P (2016) Seawater carbonate chemistry in the Bay of Villefranche, Point B (France), January2007–December 2015. Ocean Sci. Discuss. 2016: 1–43.

28. Li MC, Zeng CL, Luo SZ, Shen JN, Lin HC, Cao N (2003) Electrochemical corrosion characteristics of type 316 stainless steel in simulated anode environment for PEMFC. Electrochim. Acta, 48**:** 1735-1741

29. Fan Y, Liu W, Li S, Chowwanonthapuny T, Zhao BWY, Dong B, Zhang T, Li X (2020) Evolution of rust layers on carbon steel and weathering steel in high humidity and heat marine atmospheric corrosion. Journal of Materials Science & Technology. 39**:** 190–199

30. Cano H, Díaz I, De la Fuente D, Chico B, Morcillo M (2018) Effect of Cu, Cr and Ni alloying elements on mechanical properties and atmospheric corrosion resistance of weathering steels in marine atmospheres of different aggressivities. Mater. Corros. 69: 8–19

31. Lvovich VF (2012) Impedance spectroscopy : Application to electrochemical and dielectric phenomena. Chapter 12. John Wiley, USA.

32. Zhang X, Yang S, Zhang W, Guo H, He X (2014) Influence of outer rust layers on corrosion of carbon steel and weathering steel during wet–dry cycles. Corrosion Science, 82: 165-172

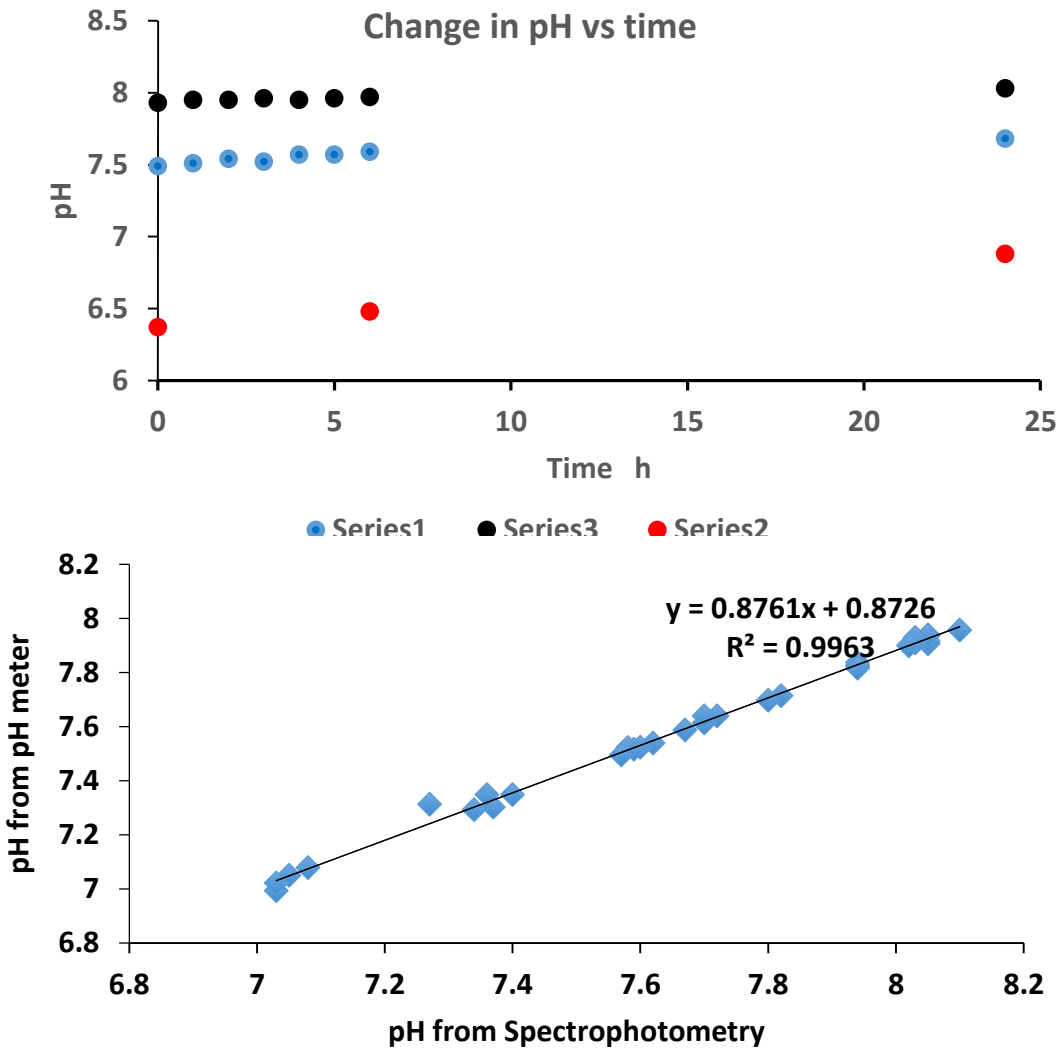

Fig 1. a) Change in pH of seawater under different pH. B) Linear relationship of the seawater pH recorded under different pH through pH meter and spectrophotometer.

A

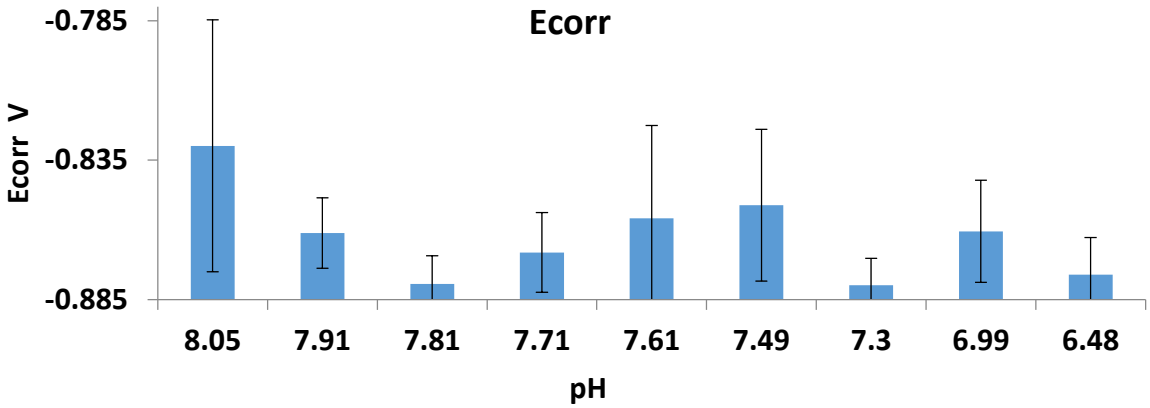
Ecorr
-0.785
-0.835
-0.885
Ecorr V
8.05
7.91
7.81
7.71
7.61
7.49
7.3
6.99
6.48
pH

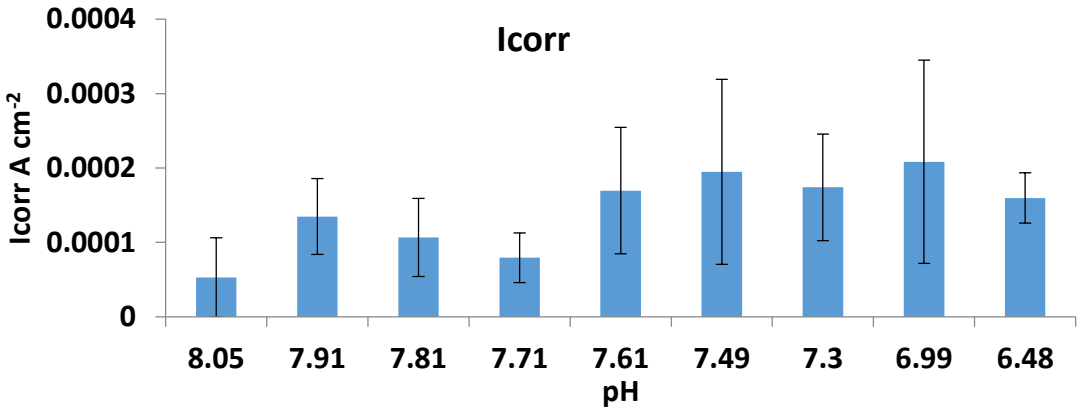
Icorr
0.0004
0.0003
0.0002
0.0001
0
Icorr A cm-2
8.05
7.91
7.81
7.71
7.61
7.49
7.3
6.99
6.48
pH

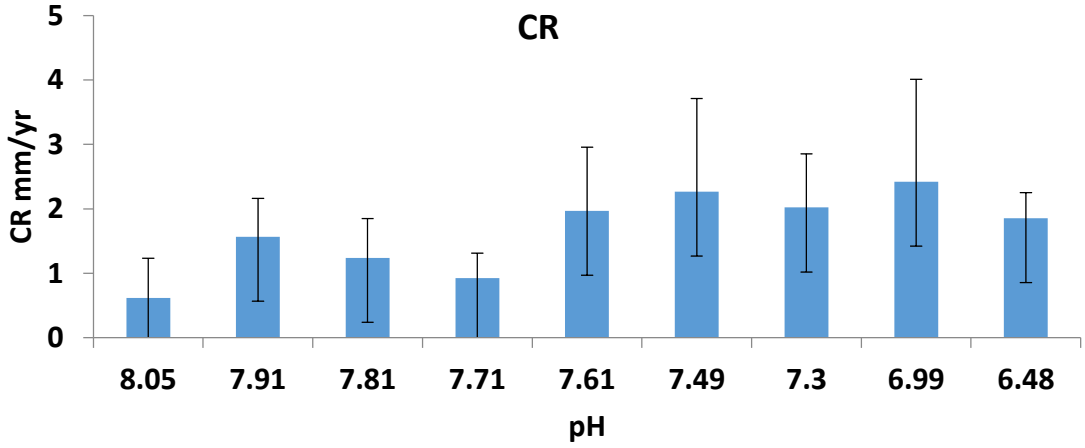
CR
5
4
3
2
1
0
CR mm/yr
8.05
7.91
7.81
7.71
7.61
7.49
7.3
6.99
6.48
pH

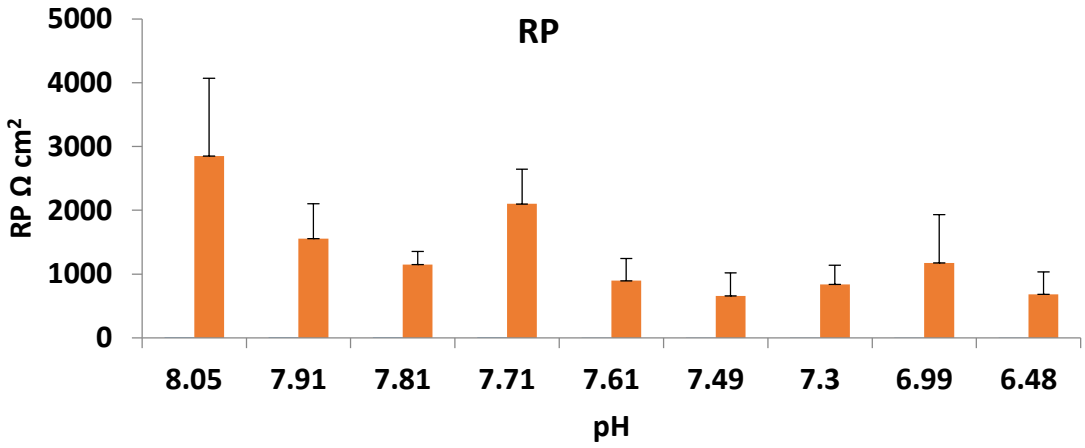

B

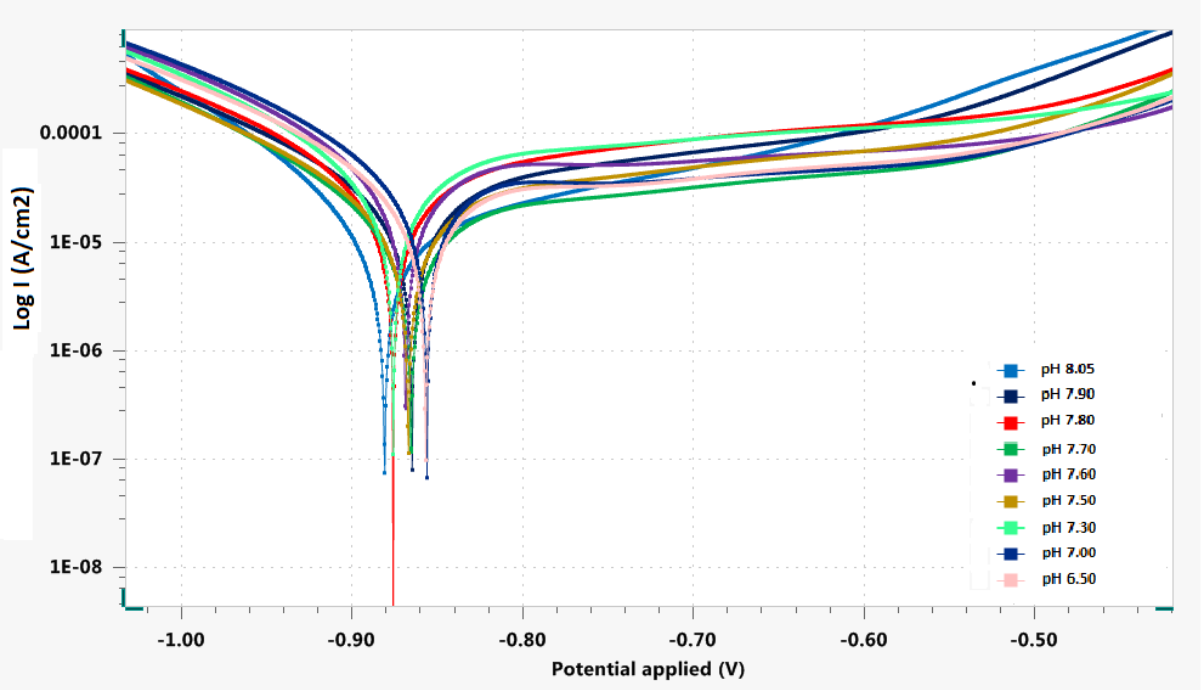

Fig 2. A) Linear sweep voltammetric data of steel under different pH conditions. B) Tafel plots of steel in different pH.

A

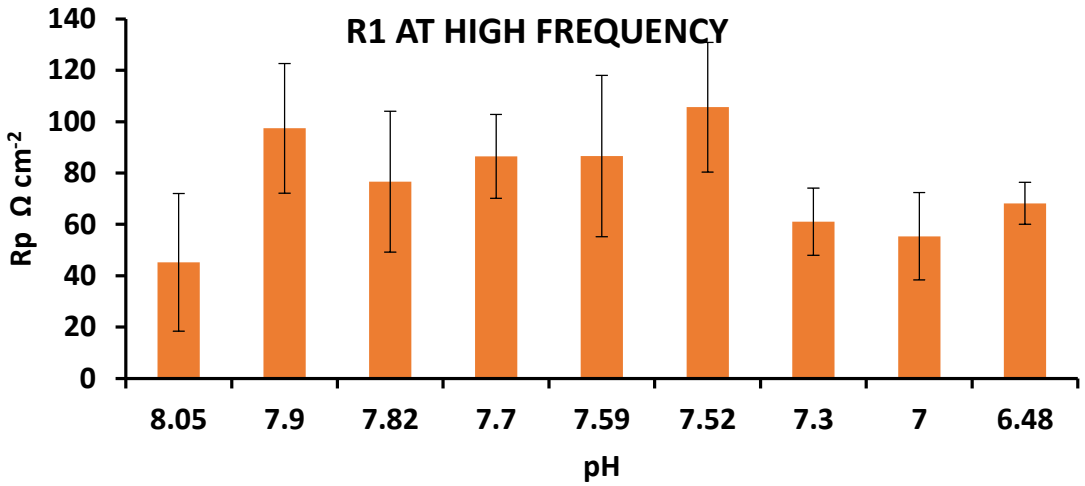
R1 AT HIGH FREQUENCY
Rp Ω cm-2
140
120
100
80
60
40
20
0
8.05
7.9
7.82
7.7
7.59
7.52
7.3
7
6.48
pH

B

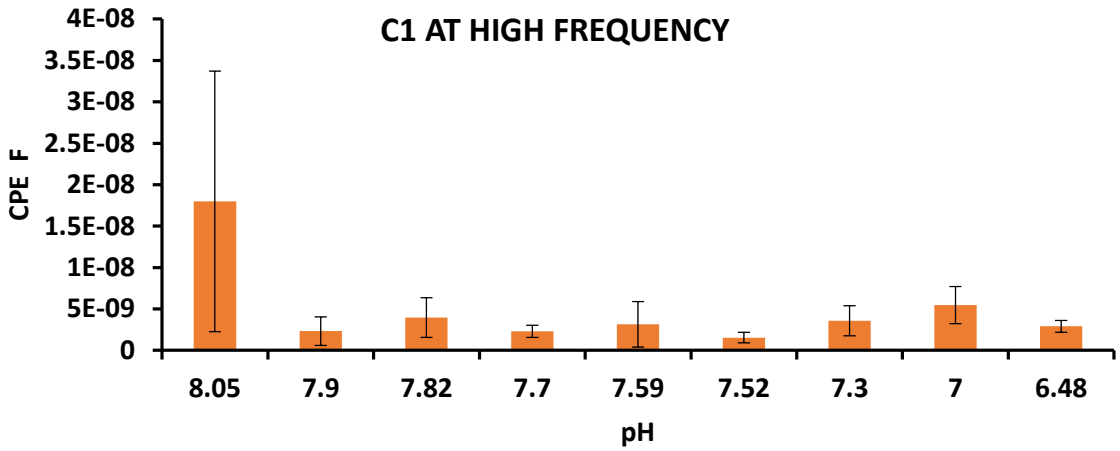
C1 AT HIGH FREQUENCY
CPE F
4E-08
3.5E-08
3E-08
2.5E-08
2E-08
1.5E-08
1E-08
5E-09
0
8.05
7.9
7.82
7.7
7.59
7.52
7.3
7
6.48
pH

C

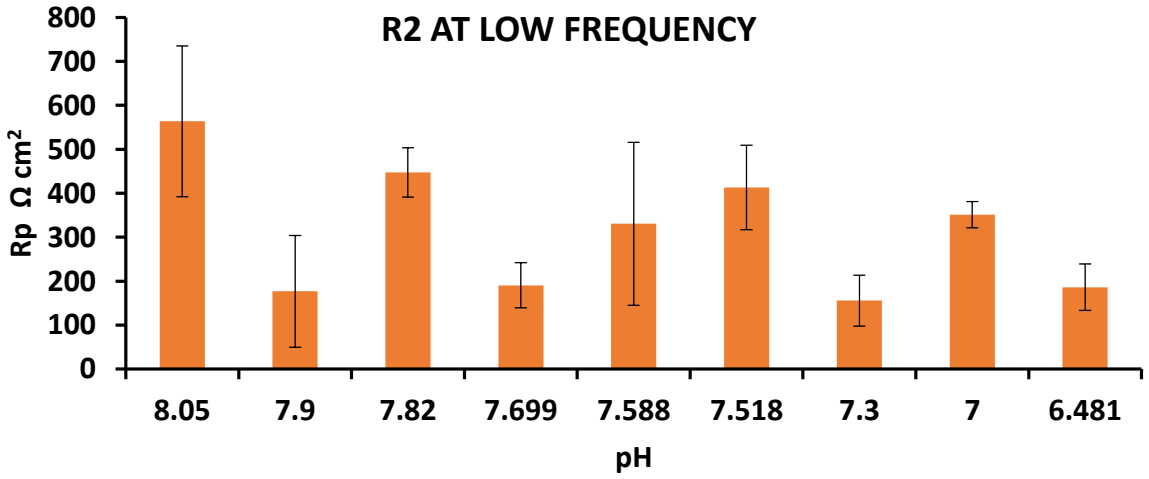
R2 AT LOW FREQUENCY
Rp Ω cm2
800
700
600
500
400
300
200
100
0
8.05
7.9
7.82
7.699
7.588
7.518
7.3
7
6.481
pH

D

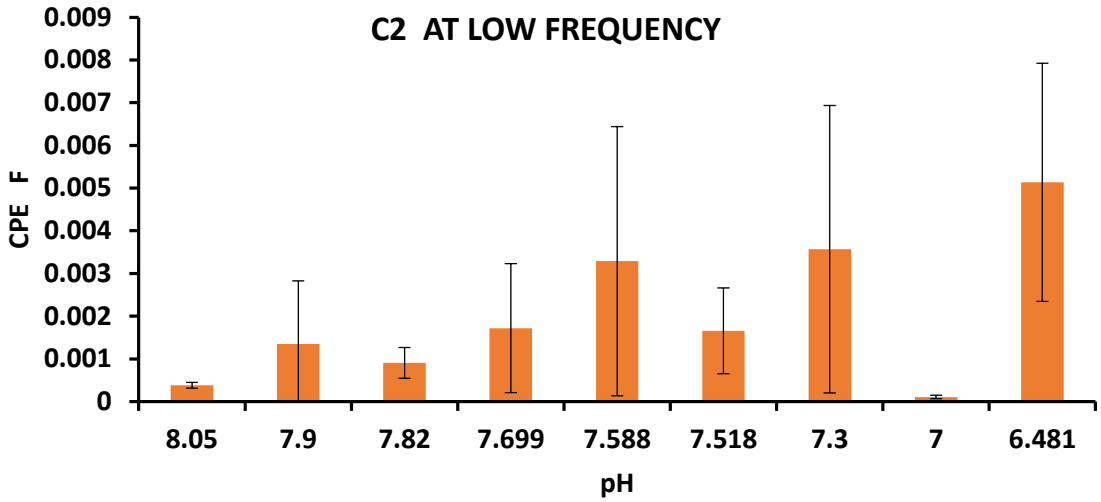
C2 AT LOW FREQUENCY
CPE F
0.009
0.008
0.007
0.006
0.005
0.004
0.003
0.002
0.001
0
8.05
7.9
7.82
7.699
7.588
7.518
7.3
7
6.481
pH

E

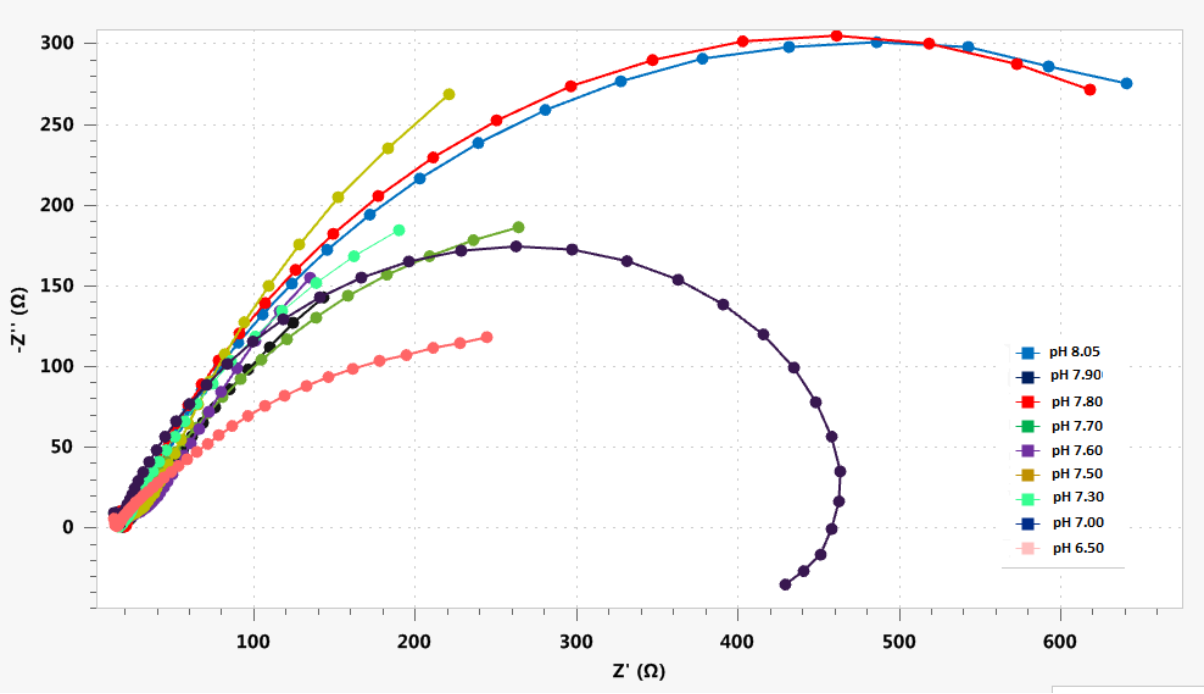
-Z'' (Ω)
300
250
200
150
100
50
0
100
200
300
400
500
600
Z' (Ω)
pH 8.05
pH 7.90
pH 7.80
pH 7.70
pH 7.60
pH 7.50
pH 7.30
pH 7.00
pH 6.50

F

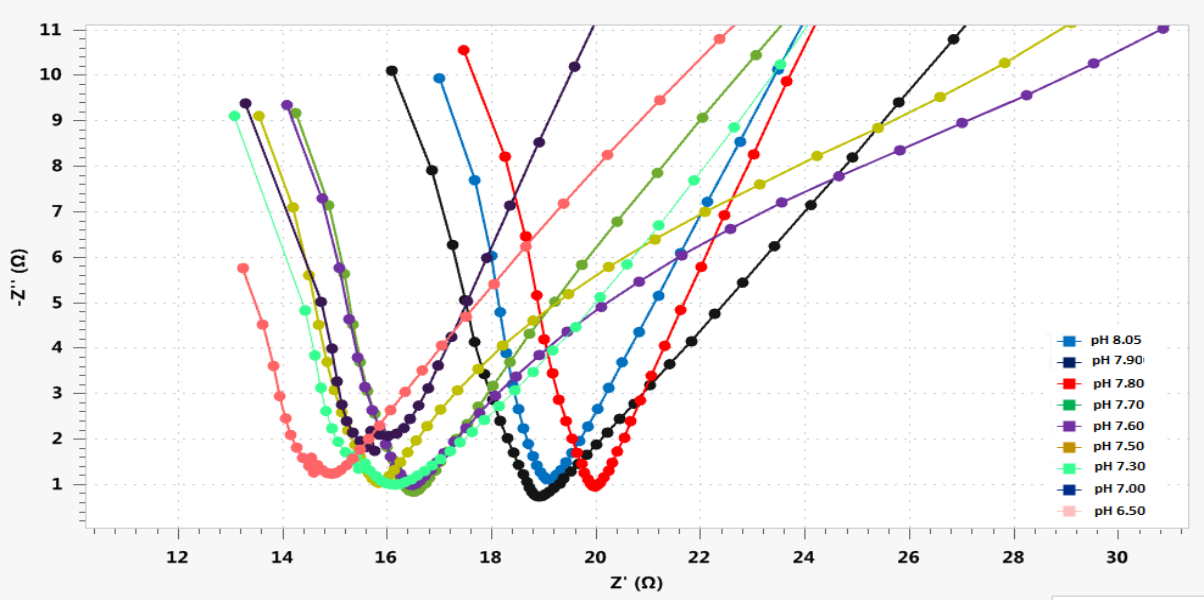

Fig 3. A to D) EIS data derived from Randles equivalent circuit model . R1 and R2 signifies the polarization resistance in the high and low frequency domains of Nyquist plot. The C1 and C2 shows the constant phase element of High and low frequency domains. E) The Nyquist plots of steel exhibit under different pH seawater. F) the high frequency domain of Nyquist plot.

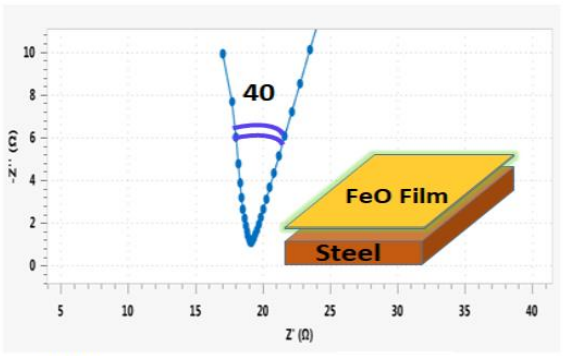

pH 8.05

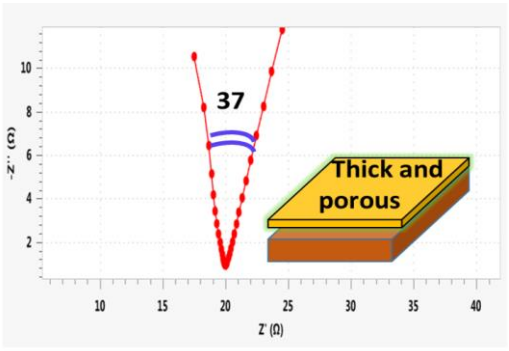

pH 7.8

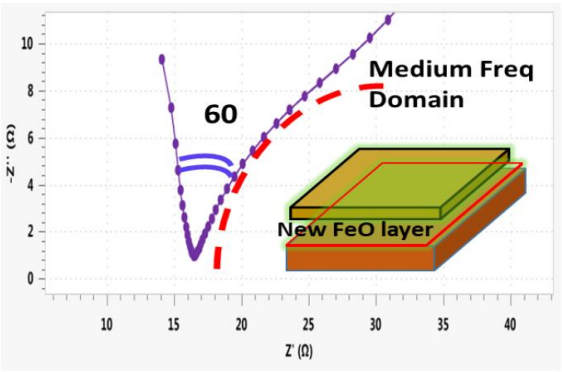

pH 7.6

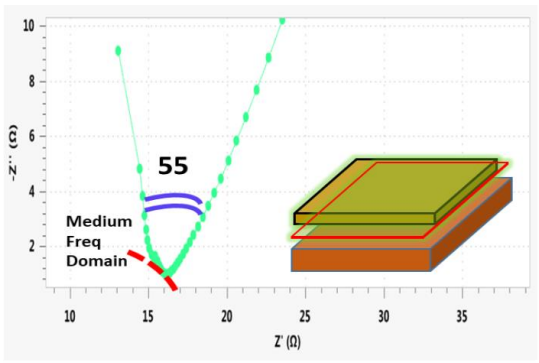

pH 7.30

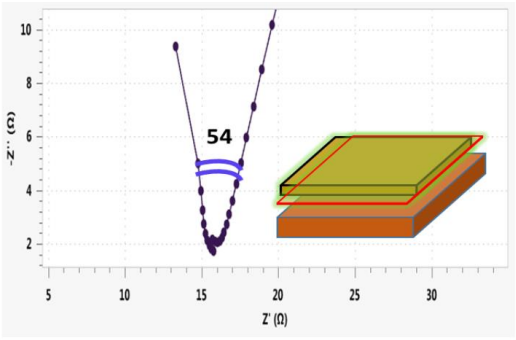

pH 7.00

Fig 4. Characterisitcs of HF domain and the behavior of steel under different pH. The redline shows the extrapolation of semi circle in the medium frequency domain

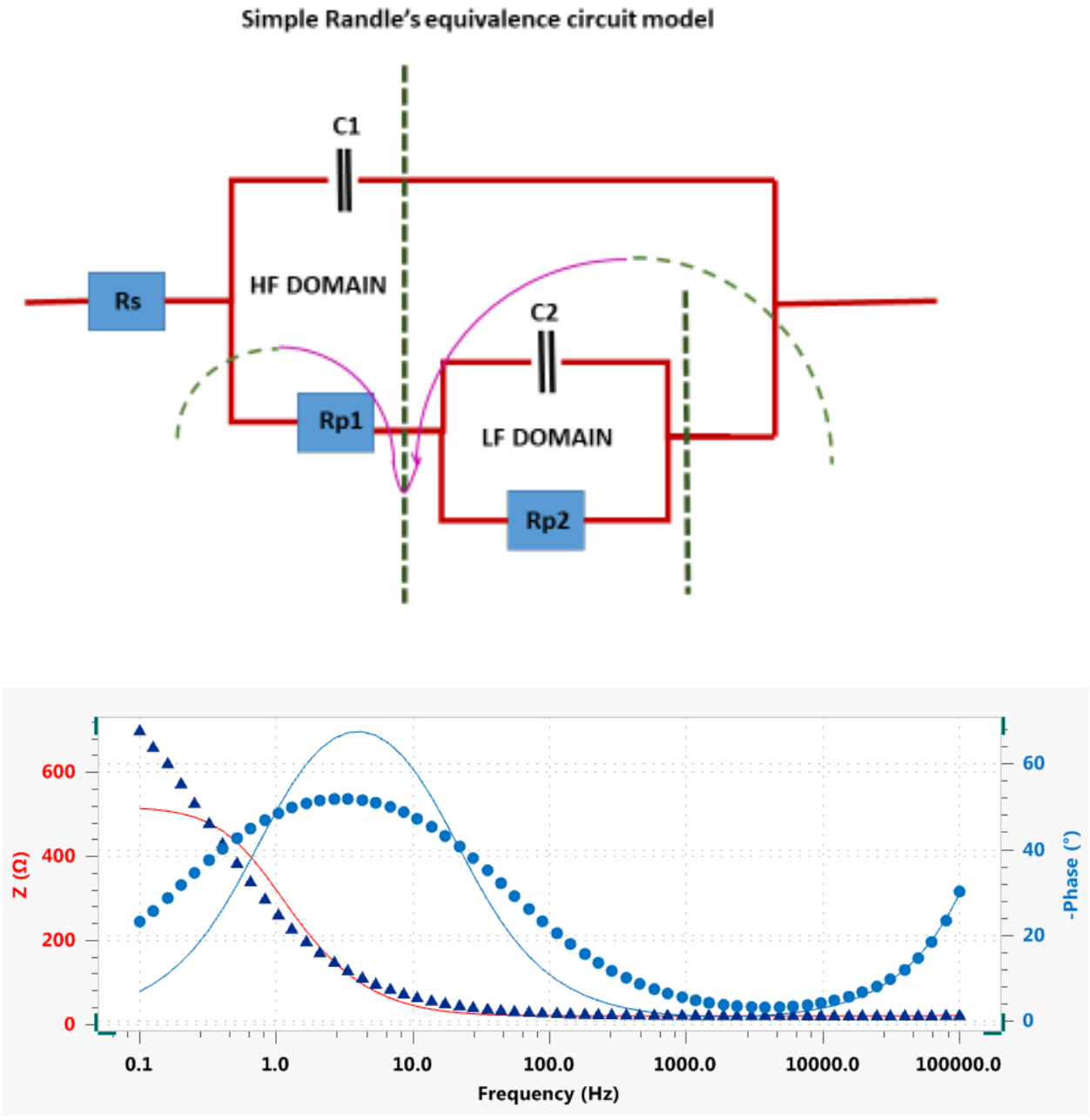

Supplementary Figure S1. A) Randle's equivalent circuit model and B) Fitted circuit in the Bode plot. The dotted line is bode curve and the line represent fitted curve as per Randle' equivalent circuit.

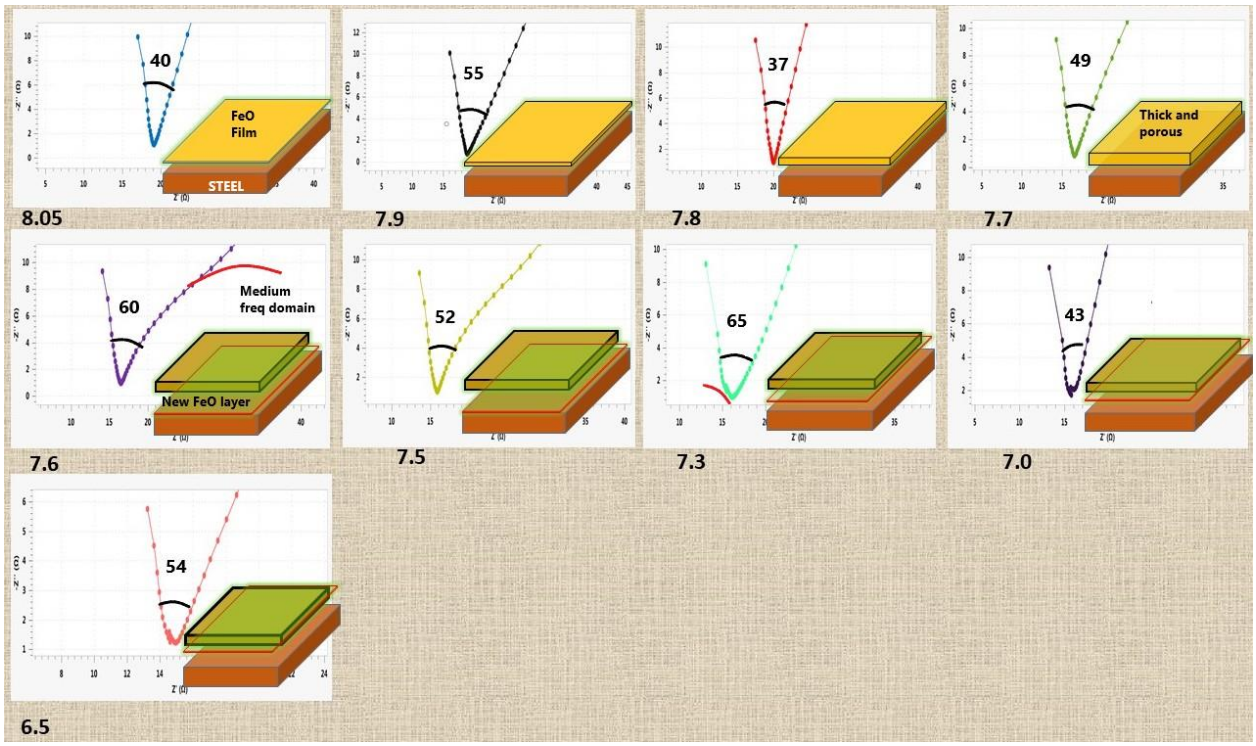

Supplementary Figure S2. Response of HF domain under varied pH.